J Nanostruct 16(1): 732-743, Winter 2026

RESEARCH PAPER

Fabrication of Zinc Oxide Nanoparticles Based on a Novel Technique of In-Liquid Plasma

Hamed Bananifard [1], *Ebrahim Nemati Lay* [1]*, *Mohsen Ashjari* [1,2]

[1] *Department of Chemical Engineering, Faculty of Engineering, University of Kashan, Kashan, 87317-53153, Iran*

[2] *Nanostructures and Biopolymers Research Lab, Institute of Nanoscience and Nanotechnology, University of Kashan, Kashan, 87317-53153, Iran*

ARTICLE INFO

Article History:
Received 04 August 2025
Accepted 24 October 2025
Published 01 January 2026

Keywords:
In-Liquid Plasma Discharge
High Voltage Current
Marx Generator
Metal Nanoparticle
Zinc Oxide

ABSTRACT

Synthesis of nanoparticles with controllable properties remains a challenge. In this study, a novel plasma discharge method in liquid was used to solve this problem along with achieving a scalable and low-cost route for nanoparticle synthesis. Here, the plasma discharge technique in liquid was used to synthesize zinc oxide (ZnO) nanoparticles. The required high voltage pulses were generated by designing a Marx generator, and the effect of varying voltages of 8000, 10000, and 12000 V on the size, shape, surface area, and crystal structure of the formed zinc oxide nanoparticles was investigated. X-ray diffraction (XRD) results confirmed the formation of a highly crystalline wurtzite phase of ZnO. Fourier transform infrared spectroscopy (FTIR) also revealed the characteristic vibrations of Zn-O. Field emission scanning electron microscopy (FESEM) micrographs showed the formation of nearly spherical and uniform particles in the range of 5-50 nm. According to the results, increasing the plasma energy resulted in a decrease in particle size and reduced agglomeration. An increase in BET surface area (S_{BET})was also observed with decreasing voltage. The specific surface area of nanoparticles formed using a voltage of 12000 reached about 99. m^2/g. Results confirmed that higher discharge voltages increase the plasma energy and produce finer particles with larger surface areas. This method offers a controllable, scalable, and environmentally friendly route to fabricate metal nanostructures with promising properties for photocatalytic and environmental applications.

How to cite this article
Banani Fard H., Nemati Lay E., Ashjari M. Fabrication of Zinc Oxide Nanoparticles Based on a Novel Technique of In-Liquid Plasma . J Nanostruct, 2026; 16(1):732-743. DOI: 10.22052/JNS.2026.01.066

INTRODUCTION

In recent decades, zinc oxide (ZnO) nanoparticles have attracted significant attention and have become an important material in various applications due to their unique optical, electronic, and physicochemical features [1]. This metal oxide nanoparticle can efficiently absorb and emit light, due to the direct band gap, approximately at about 3.37 eV at room temperature. This property makes ZnO an amazing semiconductor for various applications, including advanced photocatalytic systems to remove environmental pollutants and gas sensors to detect the harmful gases in the atmosphere [2]. In addition, the antibacterial

* *Corresponding Author Email: enemati@kashanu.ac.ir*

features of zinc oxide nanoparticles have also been considered as a promising substance for combating microbial growth and the development of antimicrobial coatings [3]. Hence, the various applications of ZnO nanostructures, including photocatalysts and gas sensors, antibacterial coatings, and optoelectronic materials, highlight their importance in both scientific research and industrial applications [4, 5].

Various methods have been developed to produce ZnO nanostructures, including wet chemical methods, chemical vapor deposition, hydrothermal, and combustion synthesis [6, 7]. However, many of these methods require hazardous chemical precursors, high temperatures, or specific controlled conditions, which limit their industrial scalability [8]. In response to these challenges, researchers are now exploring alternative methods that offer better benefits [5, 9]. In this regard, interest in physical and non-equilibrium methods, such as liquid pulse laser ablation, in liquid plasma discharge, and acoustic cavitation has increased due to their lower cost, greater safety, and more environmental compatibility [10, 11].

Although zinc oxide nanostructures have been synthesized by various methods, the liquid plasma discharge has attracted great attention. Plasma discharge in liquids using the spark or arc method is considered a novel technique for providing activation energy for the reactions at typical ambient conditions [12, 13]. In this method, electrical energy is directly applied to a localized region of the liquid, resulting in rapid evaporation and the formation of vapor bubbles [14]. Since direct phase transition from the liquid phase to the plasma phase is thermodynamically impossible, the plasma is formed in this vapor region. The active species produced by the plasma in this method include OH•, H•, and O• -, which play a key role in breaking bonds and carrying out redox and oxidation reactions [15-17]. This method allows the synthesis of nanomaterials with proper physicochemical properties and high activity, and also presents the advantages, such as control over particle size and shape, the possibility of production under a wide range of reaction conditions, and the possibility of mass production. provides [16, 18]. On the other hand, ultrasonic cavitation is also known as an effective mechanism for the production of nanostructures. The rapid collapse of created gas bubbles in the liquid phase leads to localized shocks, hot spots, and microcurrents, resulting both aid nucleation and prevent particle aggregation [18]. Therefore, it seems that combining plasma and cavitation phenomena in a reaction medium can provide more efficient and controllable synthetic processes.

In the plasma-in-liquid method, the yield of reactions and final properties of nanoparticles such as size, shape, and specific surface area are highly dependent on the design of the plasma generation device and operating conditions. The most important of these factors include discharge voltage, electrode spacing, pulse frequency and duration, electrode material and type, chemical composition, and pH of the reaction solution [19]. High discharge voltage is the main factor for plasma generation. Increasing voltage increases the energy of active species, reduces particle size, and increases the specific surface area, but at very high voltages there is a possibility of regrowth or local melting. Short, high-energy pulses also create fast vapor bubbles and stronger plasmas [20]. Also, a smaller distance between the electrodes creates a stronger electric field and easier discharge. The presence of ions (such as OH^- or NO_3^-) changes the reaction path. For example, an alkaline medium is usually more suitable for the synthesis of zinc oxide [21]. On the other hand, the type and material of the anode also affect the final properties of the nanoparticles [21, 22]. The anode can play the role of a precursor. In addition, the material of the electrode, the temperature of the solution and the electrical conductivity also affect the properties of the nanoparticles, impurities and even the efficiency of the production of nanoparticles [21].

The power supply is a critical component in the in-liquid plasma method, as the high voltage and power pulses required to generate plasma in a liquid medium can only be provided by power supplies specifically designed for this purpose [23]. The power supply must be capable of generating high-voltage pulses with controlled amplitude and frequency to provide the optimal conditions for nanoparticle synthesis control over particle size and shape, the possibility of production under a wide range of reaction conditions, and the possibility of mass production. Provides [20]. The importance of the power supply is due to the voltage and pulses produced directly affect the physical and chemical properties of the nanoparticles produced, including their size,

shape, and surface properties [24]. The use of a Marx generator as a source of high-voltage pulses that allows for the creation of very sharp, short, and frequency-controlled electrical discharges in an aqueous environment is important. This feature can create optimal conditions for the nucleation process and controlled growth of zinc oxide nanoparticles, and compared to conventional power sources, it can improve crystal quality, reduce particle aggregation, and increase specific surface area [20].

This study seeks a new method for the synthesis of ZnO nanoparticles from zinc metal electrode in aqueous medium, which is based on pulse liquid plasma discharge medium using a Marx circuit. The main challenge in plasma-in-liquid methods is to achieve scalable and energy-efficient routes for producing the nanoparticles. In this work, the effectiveness of the designed Marx generator was investigated in terms of creating very sharp and short voltage pulses in an aqueous medium. In this circuit, the capacitors are placed in parallel in the charging path and are connected in series at the moment of discharge. The result of this arrangement can be releasing the entire stored power in a short time interval and the creation of a large electric field in the electrode gap. It seems that this high-energy discharge causes rapid local evaporation, vapor bubble formation, and ultimately plasma production. After the end of the pulse, the hot bubble subsides into the cold liquid medium, and the cavitation phenomenon occurs naturally without the need for additional equipment such as ultrasonic generators or plasma jet systems.

MATERIALS AND METHODS

Chemical

Zinc wire (Diameter of 2 mm, 99.99%) and titanium wire (Diameter of 2 mm, 99.9%) were provided by Fara Pooshesh Mahoor Co. and Safir Sanat Co., respectively. Ammonia solution (NH_4OH, 25%) was purchased from Merck Co. Ethanol (C_2H_5OH, 96%) was provided by Hamoon Teb Co.

Synthesis Procedure

First, ammonia was added dropwise to 1 L of deionized water and stirred until the pH reached about 10 at room temperature. Then, a Zinc wire was used as the anode electrode, and a titanium wire was used as the cathode electrode, both located in the alkaline water. After that, a high-voltage electric current was applied to the electrodes in the water, which resulted in the production of white gel-like precipitates of zinc hydroxide. The wet precipitates were collected using filtering, washed twice with ethanol, and dried in an oven at 60 for 12 h. Dried zinc hydroxide particles were thermally treated in an oven at 400°C for 2 h, obtaining ZnO nanoparticles. Here, to investigate the effect of voltage on the surface properties, crystal structure, and particle size of nanoparticles, three ZnO nanoparticle samples were prepared using three different voltages of 8000, 10000, and 12000 V, denoted as

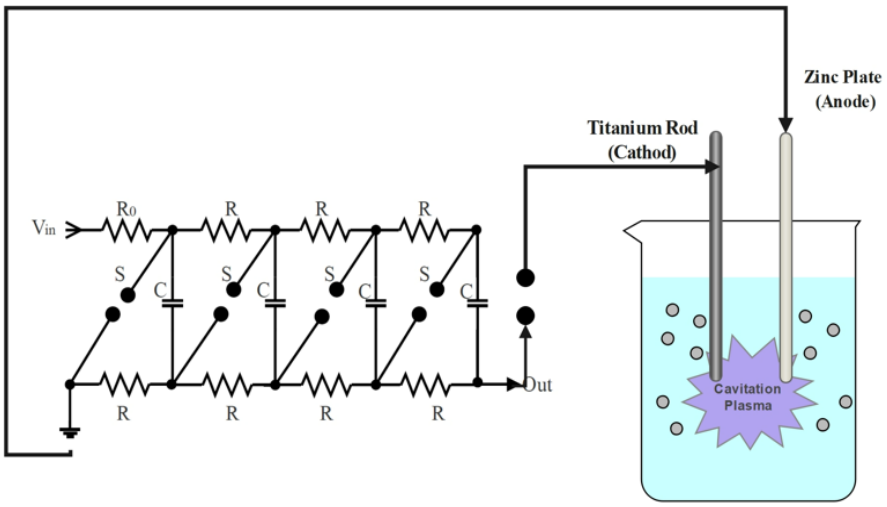

Fig. 1. Scheme of the designed Marx generator and reaction medium.

ZnO-8, ZnO-10, and ZnO-12 samples.

Here, the Marx generator was designed to produce short-time and high-voltage pulses between 2 and 14 kV in order to generate electrical discharge required in plasma synthesis. Fig. 1 presents a scheme of the designed Marx generator and reaction medium. As is clear, these capacitors were connected in series in such a way that when the circuit is activated, they create a high voltage pulse, which is necessary to create an electric discharge of plasma in the liquid medium. Each part of the Marx circuit was made using capacitors with a capacity of 10 nanofarads per stage and a voltage tolerance of up to 20 kV. The frequency of the output pulses of the Marx circuit on the pulse output and probe was measured using a digital oscilloscope with a 1:1000 high-voltage probe. The operating frequency was also recorded in the range of 7.5 Hz. The input current was 0.14 A, and the effective voltage was 220 V. The power factor of the system was considered to be nearly unity (close to 1). The nominal capacitance of the Marx circuit capacitors was confirmed to be around 40 nanofarads. The input power and energy of each pulse were calculated to be 30 W and 2 J, respectively. Given a frequency of 7.5 Hz, the pulse output power was 15 W, and consequently, the efficiency was about 50%. The spark gap distance was adjusted at about 0.8, 1, and 1.2 cm to create the high voltage discharge conditions, which resulted in the generation of high voltages at about 8000, 10000, and 12000 V, respectively.

Characterization

X-ray diffraction (XRD, PAnalytical X'Pert-Pro, Netherlands) analytical technique was used to address the crystal structure of synthesized ZnO nanoparticles, in the range of 10° to 80°. Fourier transform infrared spectroscopy (FT-IR, Magna-IR 550 spectrometer, Nicolet Co.) was applied to identify the chemical properties of samples from 400 to 4,000 cm-1. The physical properties of specific surface area, pore volume and pore size of samples were determined using Brunauer–Emmet–teller (BET) and Barrett-Joyner-Halenda (BJH) techniques, based on recorded N2 adsorption-desorption isotherms (Belsorp 28 system, Japan) using an automatic system. samples were first degassed under vacuum for 4 h at 250 °C. The field emission scanning electron microscopy (FESEM, MIRA3 TESCAN, USA) was also utilized to specify the morphology of synthesized ZnO nanoparticles. Photoluminescence spectroscopy (PL, G9800A, Agilent, USA) at room temperature, in the wavelength range of 300-700 nm, was performed to evaluate the optical properties and electron transfers in ZnO nanoparticles.

RESULTS AND DISCUSSION

The in-liquid plasma discharge method requires a stable power supply capable of generating high-voltage pulses over extended periods. The Marx circuit designed in this project was an ideal choice for creating intense electric fields due to its ability to generate powerful, short-duration pulses at sequential frequencies with high stability. Here, Under the applied discharge conditions (30 W), a representative 30-min experiment produced 2.22 g of ZnO, corresponding to a rate of about 4.4 g h^{-1}. Based on the measured mass loss of the zinc electrode and the final ZnO obtained after calcination, the reaction yield was around 94%. The corresponding energy efficiency was calculated to be approximately 148 g kWh^{-1}.

Reaction Mechanism

The mechanism of nanoparticle formation in the method performed in this study includes two stages of the creation of initial centers (nucleation) and growth, which determine the size, shape, and final properties of the nanoparticles. When plasma is created in a liquid medium under high voltage conditions, the very high temperature and pressure in the discharge zone and the rapid cooling of the surrounding environment provide completely non-equilibrium conditions. In such an environment, the released atoms and ions quickly reach a supersaturated state and tend to form initial nuclei with nanometer dimensions. These nuclei are the main base for further growth and transformation into stable nanoparticles. After the nucleation stage is completed and a significant number of stable primary nuclei are formed in the medium, the medium is no longer capable of creating new nuclei and enters the growth stage. In this stage, the growth of nanoparticles is based on the gradual attachment of ions and active species to the surface of existing nuclei. Here, Zn^{2+} ions released from the anode electrode and active oxygen species from the plasma react with the surface of the nuclei and complete the ZnO crystal lattice. In addition, the high local temperature and non-equilibrium conditions around the plasma

bubbles accelerate the diffusion process and stabilize the crystal structure.

Structural Properties

Changing the voltage in the plasma discharge process can have significant effects on the crystal structure and size of the prepared nanoparticles. The impact of voltage changes on the structural and crystalline size basic properties of the synthesized nanoparticles was investigated using X-ray diffraction analysis, as represented in Fig. 2. The diffraction peaks appeared at about 2θ values of 31°, 34°, 36°, 47°, 56.°, 63°, and 67° can be attributed to the formation of the hexagonal structure (wurtzite phase) of zinc oxide, in line with JCPDS No: 36-1451, indexed to (100), (002), (101), (102), (110), (103), and (112) plans, respectively [10, 25]. In addition, sharp and intense peaks are observed in the XRD pattern of nanoparticles, confirming the completely crystalline nature of ZnO nanoparticles [26].

ZnO is inherently a material with a stable crystalline structure. Usually, ZnO nanoparticles crystallize spontaneously even at relatively low temperatures, because the Gibbs free energy for the crystalline state is lower. There are very limited reports of the synthesis of amorphous ZnO, usually under special conditions such as chemical

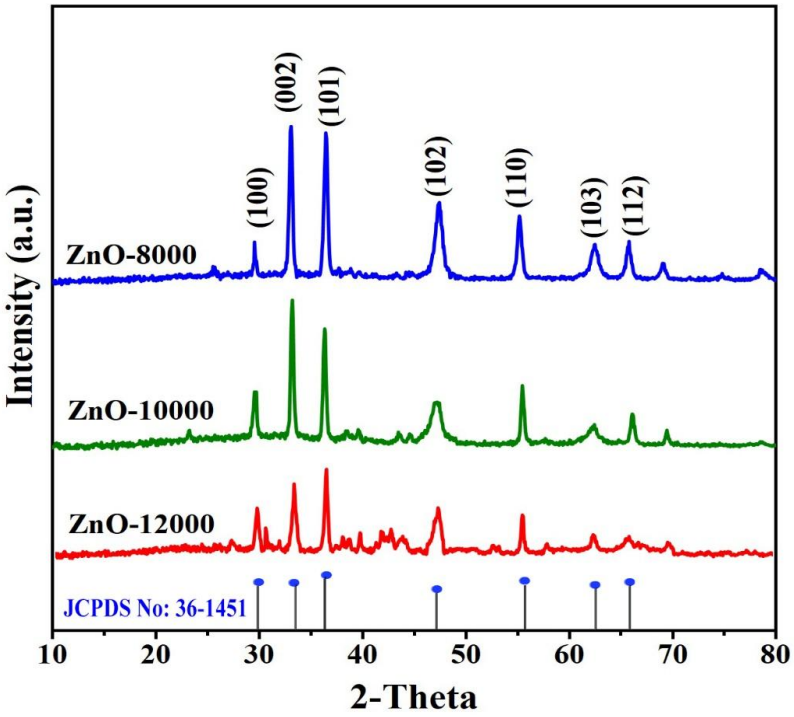

Fig. 2. XRD patterns of synthesized ZnO nanoparticle samples.

Table 1. The average crystallite size of the prepared ZnO nanoparticles using the Debye-Scherrer equation and the Williamson-Hall method.

Samples	Crystalline size (nm)	
	Debye-Scherrer	Williamson-Hall
ZnO-8000	19.6	8.7
ZnO-10000	13.3	8.7
ZnO-12000	12.3	8.7

precipitation at very low temperatures or with organic stabilizers that prevent crystallization. However, in most methods (especially plasma in a liquid, which introduces a lot of energy into the system), a completely crystalline product is obtained. ZnO nanoparticles synthesized by plasma-in-liquid discharge exhibit fully crystalline features due to the high-energy plasma environment, which provides sufficient energy for nucleation and crystal growth. Therefore, no amorphous phase is observed in the XRD patterns and the XRD patterns also confirm the absence of an amorphous background.

The average crystallite size of ZnO-8000, ZnO-10000, and ZnO-12000 was estimated based on the Debye-Scherrer equation and Williamson-Hall method, as reported in Table 1. As is clear, the sample prepared using a voltage of 12000 V (spark gap distance of 1.2 cm) led to a smaller crystallite size. In this regard, as the voltage increases, the plasma energy increases, and the atomization process intensifies. In this case, nucleation occurs more rapidly, and the crystallites have less opportunity to grow. Therefore, at higher voltages, the crystallite size and crystal defects usually reduce. This trend indicates a decrease in crystal size, which is consistent with the LaMer mechanism and an increase in the nucleation rate at intermediate voltage [25].

The results of fitting the data by the Williamson–Hall method showed that lattice strain makes a significant contribution to the peak broadening. For this reason, the crystallite sizes obtained by the Williamson–Hall method were significantly smaller than those calculated by the Debye–Scherrer equation. This is logical, since the Scherrer method assumes that all the peak broadening is due to the crystallite size, while the Williamson–Hall method attributes part of this broadening to lattice strain [27]. In both methods, a general trend of decreasing crystallite size was observed with increasing discharge voltage. The difference in the absolute value of the sizes indicates that lattice strain played a significant role in the structure of ZnO produced by the plasma method in liquid. This strain can be caused by the high growth and nucleation rate in the plasma environment, rapid changes in local temperature and pressure, and the presence of dislocations and lattice defects [28].

Chemical Properties

Fourier transform infrared spectroscopy (FTIR) was used as a powerful tool for identifying the

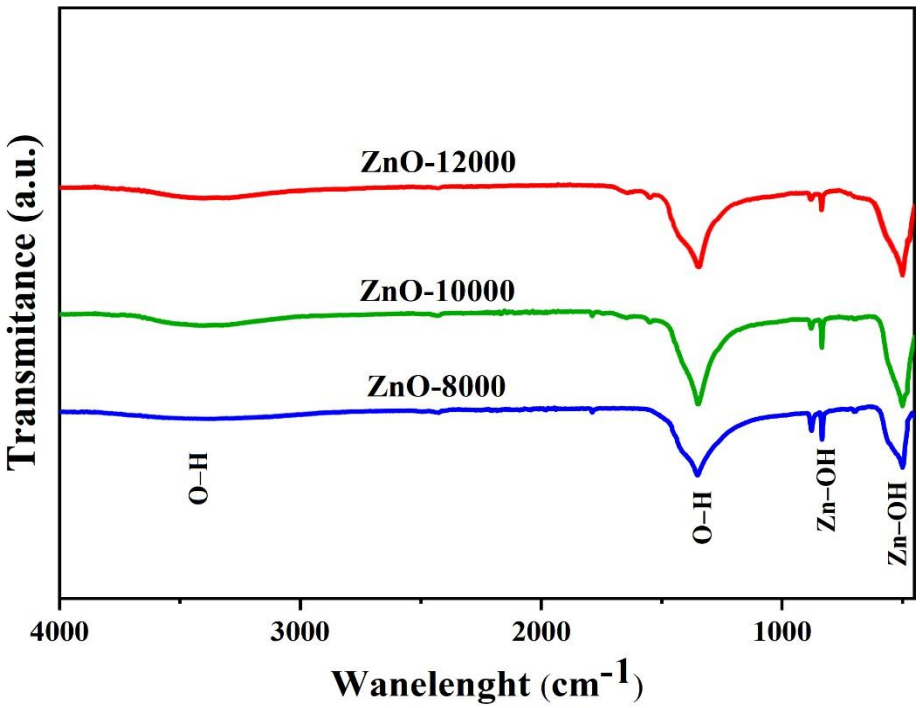

Fig. 3. FTIR spectra of synthesized ZnO nanoparticle samples.

functional groups and chemical bonds in the synthesized zinc oxide nanoparticles. According to the FTIR results in Fig. 3, the sharp absorption band observed around 500 cm^{-1} refers to the vibrations of zinc–oxygen (Zn–O) bonds, which is the most important indication for the synthesis of zinc oxide [29]. The broad absorption bands around 3300-3500 cm^{-1} as well as around 1350 cm^{-1} corresponded to the vibration of hydroxyl (OH) groups on the surface of nanoparticles, which is caused by the absorption of water molecules and surface moisture [30]. The peaks at the 1386 cm^{-1} may also be due to oxygen vacancies, which are characterized as hydrogen-related defects on the surface of ZnO in wurtzite hexagonal type ZnO crystals [31]. In addition, the sharp peaks that appeared at around 830 cm^{-1} can be attributed to the Zn-OH bonds [32].

Morphology and Physical Properties

The morphology of ZnO-8000, ZnO-10000, and ZnO-12000 nanoparticles, including shape, size, uniformity, porosity degree, surface roughness, and agglomeration of particles, which is of immense importance in the nanoparticle synthesis field, was evaluated using the FE-SEM micrographs, represented in Fig. 4. As is clear, the formation of spherical particles with almost uniform dimensions in the range of 5 to 50 nm can be observed for all prepared ZnO nanoparticles. The amount of voltage in the liquid plasma discharge method has a direct effect on particle size and particle shape. Here, it is observed that increasing the voltage led to a decrease in the particle size. In the plasma discharge method, local temperatures increase, and rapid cooling occurs. Therefore, a porous structure is obtained for the

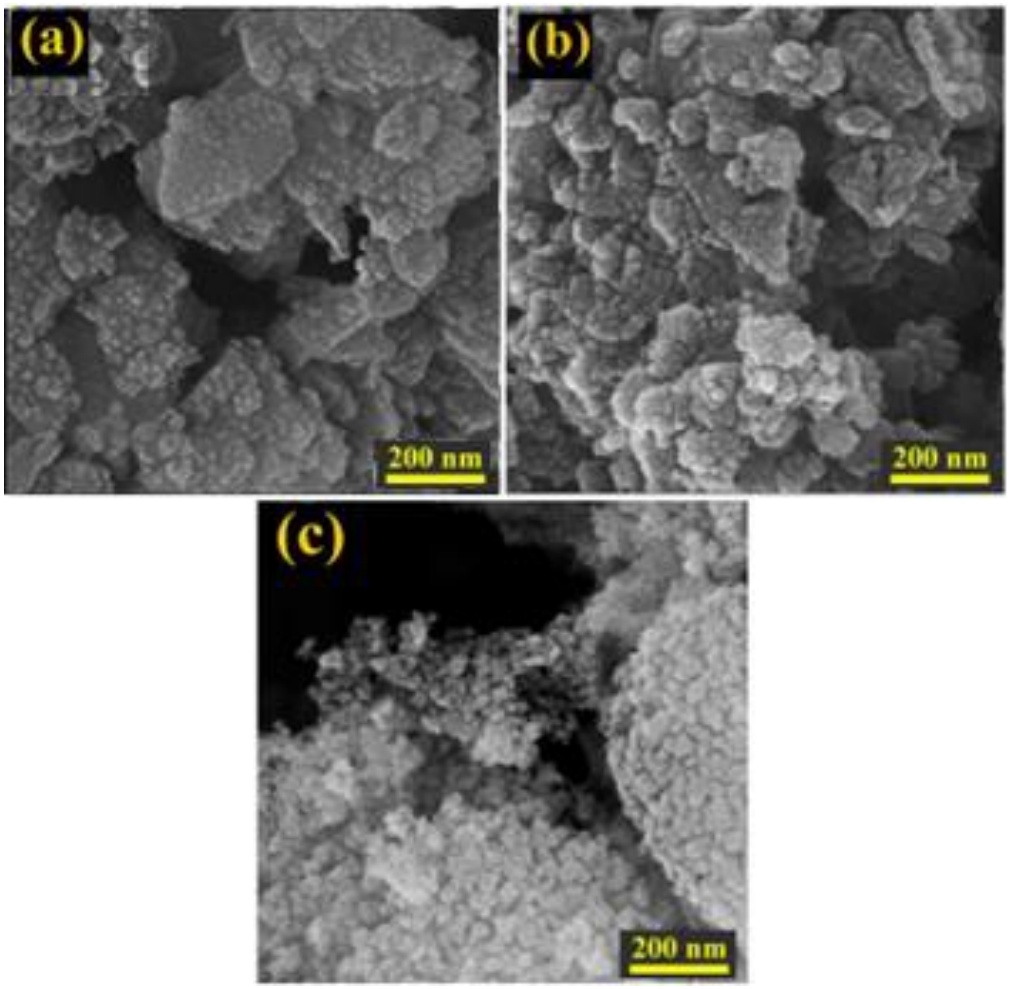

Fig. 4. FE-SEM micrographs of (a) ZnO-8000, (b) ZnO-10000, and (c) ZnO-12000 nanoparticles.

synthesized nanoparticles [33]. Furthermore, the particle size formed in the sample with a voltage of 12,000 (ZnO-12000) is clearly smaller than ZnO-10000, and ZnO-8000 and has much less agglomeration. Increasing the voltage can causes the agglomerates to break, which reduces the particle size [15].

Although increasing the voltage can reduce the initial particle size, at very high voltages, high local temperatures may cause local melting and coalescence of the particles, subsequently leading to agglomeration or increased particle size and non-uniformity. It is also possible to change the morphology from perfectly spherical particles to rod-like or sheet-like shapes, depending on the plasma energy [15].

The specific surface area, pore volume, and pore diameters have a direct relationship with the performance of ZnO nanoparticles, especially in photocatalytic applications [34]. Higher specific surface area means more active sites for adsorbing pollutant molecules. Table 2 indicates the specific surface area, mean pore size, and pore volume of the ZnO-8000, ZnO-10000, and ZnO-12000 samples. As is clear, increasing the voltage from 8000 to 10000 and 12000 V led to an increase in the surface area from 71 m^2/g up to 94 and 99 m^2/g, respectively. In addition, the mean pore diameters were also decreased with increasing voltage. It seems that with increasing the spark gap distance and consequently the voltage, more plasma energy is generated and atomization occurs more strongly, leading to the formation of finer particles and a higher specific surface area [35, 36]. Furthermore, the high voltage created in-liquid plasma discharge also leads to the breakdown of agglomerates and increases the effective specific surface area of the nanoparticles [37, 38].

However, it is observed that increasing the voltage from 10000 to 12000 did not lead to a significant improvement in the specific surface

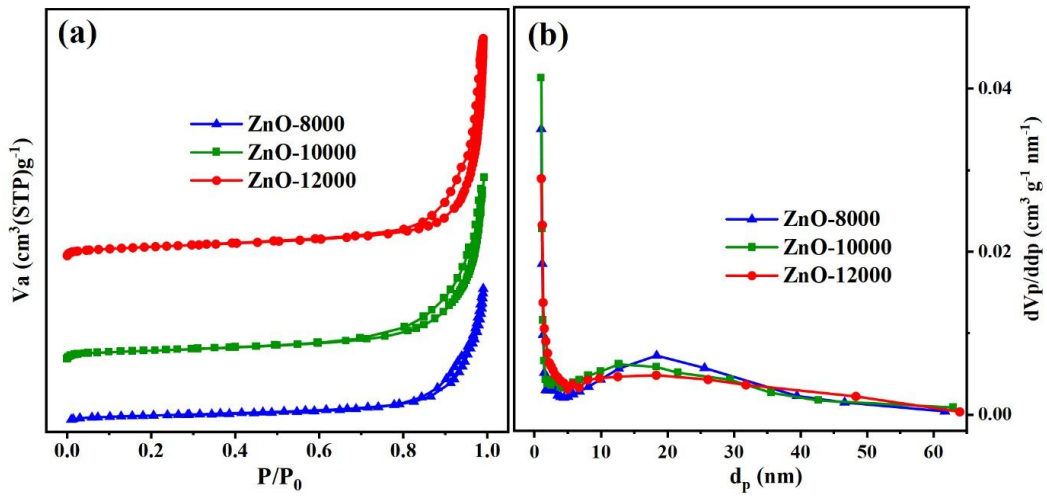

Fig. 5. The nitrogen adsorption-desorption isotherms, and (b) pore size distribution of the prepared ZnO nanoparticles.

Table 2. Specific surface area, mean pore size, and total pore volume of the prepared nanoparticles.

Samples	Specific Surface Area (m^2/g)	Mean Pore Size (nm)	Total Pore Volume (cm^3/g)
ZnO-8000	71	11.3	0.49
ZnO-10000	94	8.9	0.65
ZnO-12000	99	8.1	0.81

area. At very high voltages, particle growth may reach equilibrium, which limits the increase in specific surface area. Also, at high voltages, some of the micropores may disappear or coalesce to form larger mesopores, resulting in a less-than-expected increase in specific surface area [17, 39].

Fig. 5a represents the N_2 adsorption-desorption isotherms of the prepared ZnO nanoparticles. The adsorption isotherms of all nanoparticles correspond to type IV according to the IUPAC standard classification, indicating mesopore structures with interconnected pores [40]. The type IV isotherm is usually associated with a rapid increase in N_2 adsorption at high relative pressures and shows a hysteresis loop in the adsorption-desorption isotherm, as is clear in Fig. 5a The hysteresis loops in ZnO nanoparticles refer to type H-3, representing the presence of open pores in their structures [41].

Fig. 5b indicates the pore size distribution of the prepared ZnO nanoparticles, based on the BJH technique. The results confirm the formation of mesopores in the range of 2-50 nm. The formation of nanoparticles with a mesopore structure and relatively high specific surface area is ideal for photocatalytic applications [42]. In the plasma discharge method, the nanoparticles are usually formed as mesopores because rapid crystal growth is accompanied by the creation of interparticle spaces.

Optical properties

Photoluminescence spectroscopy is one of the key methods in identifying energy band characteristics, determining the band gap, and also detecting trap states and crystal defects in nanostructures. Since the photocatalytic performance of ZnO nanoparticles is strongly affected by electron-hole recombination and the presence of defect centers, the use of photoluminescence testing allows for indirect evaluation of the photocatalytic efficiency of samples [43]. Fig. 6 indicates the PL spectrum of the ZnO=12000 sample. As can be seen, three distinct bands are observed, each representing electron-hole recombination processes at different energy levels and the presence of various crystal/surface defects [44]. The peak around 396 nm can be

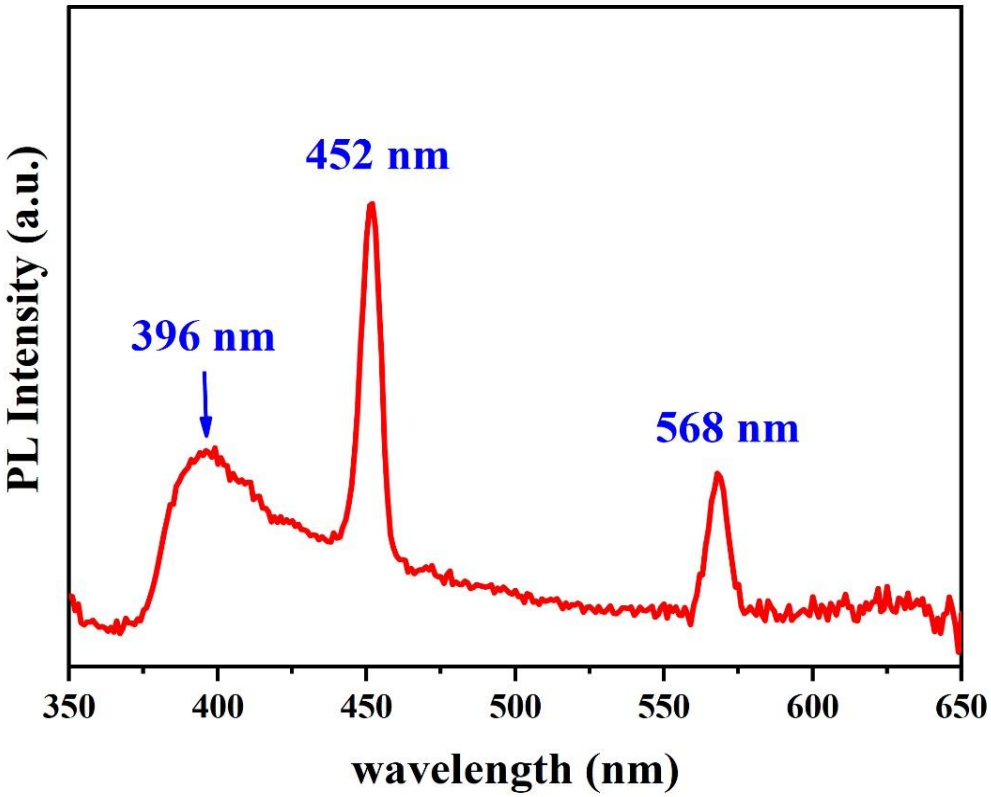

Fig. 6. Optical properties of the prepared ZnO nanoparticles.

attributed to near-band edge emission; this peak indicates radiative recombination of conduction band electrons with valence band holes, and its presence indicates the presence of a significant fraction of relatively good crystallinity in the sample [45]. The sharp peak around 452 nm (blue region) is usually attributed to emission associated with shallow donor surfaces or interband states due to interstitial zinc atoms (Zn_i) or deep surface-half transitions.

The peak around 568 nm (orange/yellow) represents emission due to oxygen vacancies, oxygen interstitials or deep surface trap centers, which usually indicate the presence of bulk defects or oxide surface adsorptions and are known as surface-repulsion emissions [46]. The relatively good intensity of the peak (396 nm) indicates a high ratio of radiative recombination and acceptable crystal quality. The blue peak (452 nm) with significant intensity indicates that the sample has a certain number of surface/interstitial conduction carriers that can affect the photocatalytic behavior, for example, they can facilitate charge separation or change recombination pathways [45, 46].

Comparison with Previous Studies

Recently, many attempts have been made to produce nanoparticles using plasma technology, and many reports have also described the optimal operating conditions required for plasma production and the various mechanisms for producing nanoparticles. Table 3 provides a brief comparison between the findings of this study and previous reports on the preparation of zinc oxide nanoparticles using plasma technology. Abdullah EA et al [47] produced the ZnO nanoparticles in spherical particles with particle size of 10-50 nm using atmospheric plasma jet method, and funded that the morphology is completely dependence on concentration of NaOH–HNO_3 solution. In study conducted using microwave plasma in liquid [48], nanoparticles with metallic zinc were formed in hexagonal and cylindrical shapes with particle sizes of about 10-200 nanometers. Saito et al [49] was also investigated the effect of differnte voltages ranging 42-200 V in soluble plasma method on synthesis of ZnO nanoparticles using zinc wire as cathode, and potassium carbonate solution. The resulted nanoparticles were obtained in nanoflowers and nanorods morphology with particle size of less than 100 nm.

The proposed method in the present study, with a strong discharge by a Marx generator designed, produces extremely high pulse energy for plasma generation. This method is expected to have higher energy efficiency than conventional continuous discharges. The nanoparticles produced in this research have also been produced with spherical

Table 3. Comparison between the preparation method of zinc oxide nanoparticles using plasma technology.

Plasma type	Chemical & medium	Operating conditions	Morphology	Particle size	Advantages/ Disadvantage	Ref
Marx Generator	Zinc electrode, Liquid Medium	12000 V pH: 10	spherical & uniform particles	< 50 nm	Strong pulses, 94% efficiency	Current study
Atmospheric plasma jet	Zinc sheet NaOH–HNO_3 solution, water argon flow	~3 kV AC 40 kHz ~30 W	spherical particles	10-50 nm	Morphology dependence on concentration.	[47]
Microwave plasma in liquid	Zinc electrode, Ethanol, Water	microwave of 250 W	hexagonal & cylinders Particles	10-200 nm	production rate of 3.3 g/h. Zn impurity	[48]
Soluble plasma	zinc wire (cathode), K_2CO_3 solution	voltages of 42 to 200 V	nanoflowers nanorods	<100 nm	control morphology with power. melting of cathode with high voltage	[49]

and uniform morphology with dimensions less than 50 nm.

CONCLUSION

The successful synthesis of zinc oxide nanoparticles was investigated using a novel plasma discharge method in liquid, and the effect of voltage changes was investigated through spark gap changes. In this study, a Marx generator was designed to generate high voltage and short-duration pulses. The formation of zinc oxide wurtzite structure was confirmed in all samples, so that the average crystallite size of the ZnO sample provided using a voltage of 12 kV was reached at about 17 nm. The size of ZnO crystals synthesized by the liquid plasma discharge method was calculated using the Debye-Scherer equation and the Williamson-Hall method. The results of both methods showed that increasing the discharge voltage leads to a decrease in crystal size." The FESEM micrographs confirmed the formation of spherical particles with almost uniform dimensions in the range of 5 to 50 nm. The FESEM results also showed decreasing particle size and reduced agglomeration with increasing discharge voltage. Also, more uniform and porous nanostructures were obtained by using a higher voltage. However, the results confirmed that although increasing the plasma energy from 8 to 12 kV leads to an increase in the specific surface area from 71 m^2/g up to 99 m^2/g, an excessive increase may not have much effect on the specific surface area or even have the opposite result. The outcomes indicate that the plasma discharge method in liquid can enable the synthesis of active nanoparticles with suitable properties, along with controlling the size and porosity of the particles through voltage control, without the use of hazardous precursors or auxiliary equipment such as ultrasonics. This flexibility, along with the elimination of dissolved precursors and extraneous gases, makes the present method a suitable option for producing ZnO nanostructures on both a laboratory and semi-industrial scale.

CONFLICT OF INTEREST

The authors declare that there is no conflict of interests regarding the publication of this manuscript.

REFERENCES

1. Zhu C, Wang X. Nanomaterial ZnO Synthesis and Its Photocatalytic Applications: A Review. Nanomaterials. 2025;15(9):682.
2. Ali H, Guler AC, Masar M, Antos J, Hanulikova B, Urbanek P, et al. Structural factors influencing photocatalytic and photoelectrochemical performance of low-dimensional ZnO nanostructures. Catal Today. 2025;445:115088.
3. Hao Y, Wang Y, Zhang L, Liu F, Jin Y, Long J, et al. Advances in antibacterial activity of zinc oxide nanoparticles against Staphylococcus aureus (Review). Biomedical Reports. 2024;21(5).
4. Prashanth GK, Dileep MS, Gadewar M, Ghosh MK, Rao S, Giresha AS, et al. Zinc Oxide Nanostructures: Illuminating the Potential in Biomedical Applications: a Brief Overview. BioNanoScience. 2024;14(2):1876-1896.
5. Raha S, Ahmaruzzaman M. ZnO nanostructured materials and their potential applications: progress, challenges and perspectives. Nanoscale Advances. 2022;4(8):1868-1925.
6. Svoboda L, Dvorský R, Praus P, Matýsek D, Bednář J. Synthesis of ZnO nanocoatings by decomposition of zinc acetate induced by electrons emitted by indium. Appl Surf Sci. 2016;388:491-496.
7. Noman MT, Amor N, Petru M. Synthesis and applications of ZnO nanostructures (ZONSs): a review. Crit Rev Solid State Mater Sci. 2021;47(2):99-141.
8. Wee BS, Droepenu EK, Chin SF, Kok KY, Ting W. Variation of Alkali Concentration and Temperature: Its Effect on the Morphology of ZnO Nanoparticles Synthesized via Solvothermal Technique. Defect and Diffusion Forum. 2021;411:3-15.
9. Hasnidawani JN, Azlina HN, Norita H, Bonnia NN, Ratim S, Ali ES. Synthesis of ZnO Nanostructures Using Sol-Gel Method. Procedia Chemistry. 2016;19:211-216.
10. Imran HJ, Hubeatir KA, Aadim KA. A novel method for ZnO@NiO core–shell nanoparticle synthesis using pulse laser ablation in liquid and plasma jet techniques. Sci Rep. 2023;13(1).
11. Bulychev NA. Obtaining Nanosized Materials in Plasma Discharge and Ultrasonic Cavitation. High Temperature. 2022;60(S1):S98-S126.
12. Primc G, Brenčič K, Mozetič M, Gorjanc M. Recent Advances in the Plasma-Assisted Synthesis of Zinc Oxide Nanoparticles. Nanomaterials. 2021;11(5):1191.
13. Bounedjar N, Ferhat MF, Toukal L, Messai R. Non thermal plasma synthesis of ZnO nanoparticles and their corrosion inhibition activity on XC70 mild steel pipeline in 1 M HCl acidic medium. Materials Chemistry and Physics. 2024;311:128555.
14. Kang J, Li OL, Saito N. Synthesis of structure-controlled carbon nano spheres by solution plasma process. Carbon. 2013;60:292-298.
15. Bulychev NA. Study of Interaction of Surface-Active Polymers With Zinc Oxide Nanoparticles Synthesized In Ultrasonically Assisted Plasma Discharge. Nanoscience and Technology: An International Journal. 2022;13(1):55-65.
16. Chen Q, Li J, Li Y. A review of plasma–liquid interactions for nanomaterial synthesis. J Phys D: Appl Phys. 2015;48(42):424005.
17. Bruggeman PJ, Bogaerts A, Pouvesle JM, Robert E, Szili EJ. Plasma–liquid interactions. J Appl Phys. 2021;130(20).
18. Khatoon N, Yasin HM, Younus M, Ahmed W, Rehman NU, Zakaullah M, et al. Synthesis and spectroscopic characterization of gold nanoparticles via plasma-liquid interaction technique. AIP Advances. 2018;8(1).
19. Jyoti Boruah P, Kalita P, Bailung H. In-Liquid Plasma: A Novel Tool for Nanofabrication. Plasma Science and Technology: IntechOpen; 2022. http://dx.doi.org/10.5772/

intechopen.98858
20. Locke BR, Thagard SM. Analysis and Review of Chemical Reactions and Transport Processes in Pulsed Electrical Discharge Plasma Formed Directly in Liquid Water. Plasma Chem Plasma Process. 2012;32(5):875-917.
21. Bai F, Yan A, Fu Y, Khan I, Huang Y, Cao F, et al. Acoustic Cavitation-Assisted Plasma Generation in Liquid Media. Advanced Materials Technologies. 2025;10(16).
22. Vanraes P, Bogaerts A. Plasma physics of liquids—A focused review. Applied Physics Reviews. 2018;5(3).
23. Horikoshi S, Serpone N. In-liquid plasma: a novel tool in the fabrication of nanomaterials and in the treatment of wastewaters. RSC Adv. 2017;7(75):47196-47218.
24. Locke BR, Thagard SM, Lukes P. Recent Insights Into Interfacial Transport and Chemical Reactions of Plasma-Generated Species in Liquid. Plasma Processes and Polymers. 2024;22(1).
25. Marković S, Stojković Simatović I, Ahmetović S, Veselinović L, Stojadinović S, Rac V, et al. Surfactant-assisted microwave processing of ZnO particles: a simple way for designing the surface-to-bulk defect ratio and improving photo(electro) catalytic properties. RSC Advances. 2019;9(30):17165-17178.
26. S M, N H, P.P V. In Vitro Biocompatibility and Antimicrobial activities of Zinc Oxide Nanoparticles (ZnO NPs) Prepared by Chemical and Green Synthetic Route— A Comparative Study. BioNanoScience. 2019;10(1):112-121.
27. Mote VD, Purushotham Y, Dole BN. Williamson-Hall analysis in estimation of lattice strain in nanometer-sized ZnO particles. Journal of Theoretical and Applied Physics. 2012;6(1).
28. Paul P, Robel FN, Bahadur NM, Tabassum S, Dey SS, Bashar MS, et al. Crystallographic facet engineering of ZnO nanoparticles for photocatalytic organic pollutant degradation and antibacterial activity. Materials Advances. 2025;6(14):4696-4704.
29. Messai R, Ferhat MF, Belmekki B, Alam MW, Al-Othoum MAS, Sadaf S. GAD plasma-assisted synthesis of ZnO nanoparticles and their photocatalytic activity. Materials Research Express. 2024;11(1):015006.
30. Parlakyigit AS, Ergun C, Gokcekaya O. Synthesis of ZnO nanoparticles via spray atomization assisted inductively coupled plasma technique. Ceram Int. 2023;49(14):23035-23044.
31. Wei SF, Lian JS, Jiang Q. Controlling growth of ZnO rods by polyvinylpyrrolidone (PVP) and their optical properties. Appl Surf Sci. 2009;255(15):6978-6984.
32. Balogun SW, James OO, Sanusi YK, Olayinka OH. Green synthesis and characterization of zinc oxide nanoparticles using bashful (Mimosa pudica), leaf extract: a precursor for organic electronics applications. SN Applied Sciences. 2020;2(3).
33. Anwar M, Saraswati TE, Anjarwati L, Moraru D, Udhiarto A, Adriyanto F, et al. Probing ionization characteristics of under-water plasma arc discharge using simultaneous current and voltage versus time measurement in carbon nanoparticle synthesis. Micro and Nano Engineering. 2022;14:100099.
34. Pujara A, Sharma R, Samriti, Bechelany M, Mishra YK, Prakash J. Novel zinc oxide 3D tetrapod nano-microstructures: recent progress in synthesis, modification and tailoring of optical properties for photocatalytic applications. Materials Advances. 2025;6(7):2123-2153.
35. Burakov VS, Nevar EA, Nedel'ko MI, Tarasenko NV. Synthesis and modification of molecular nanoparticles in electrical discharge plasma in liquids. Russ J Gen Chem. 2015;85(5):1222-1237.
36. Wang J, Zhang W, Wu T, Chen M, Dong M. Occurrence of giant plasma bubble in liquid. Matter. 2024;7(9):3024-3035.
37. Saito G, Akiyama T. Nanomaterial Synthesis Using Plasma Generation in Liquid. Journal of Nanomaterials. 2015;2015(1).
38. Patel J. A Commentary on the Plasma-Liquid Interactions. Russian Journal of Physical Chemistry B. 2024;18(5):1301-1308.
39. Kovačević VV, Sretenović GB, Obradović BM, Kuraica MM. Low-temperature plasmas in contact with liquids—a review of recent progress and challenges. J Phys D: Appl Phys. 2022;55(47):473002.
40. Zhao A, Ying W, Zhang H, Ma H, Fang D. Ni–Al2O3 catalysts prepared by solution combustion method for syngas methanation. Catal Commun. 2012;17:34-38.
41. Xu L, Zhang J, Ding J, Liu T, Shi G, Li X, et al. Pore Structure and Fractal Characteristics of Different Shale Lithofacies in the Dalong Formation in the Western Area of the Lower Yangtze Platform. Minerals. 2020;10(1):72.
42. Hussain RT, Hossain MS, Shariffuddin JH. Green synthesis and photocatalytic insights: A review of zinc oxide nanoparticles in wastewater treatment. Materials Today Sustainability. 2024;26:100764.
43. Saikia L, Bhuyan D, Saikia M, Malakar B, Dutta DK, Sengupta P. Photocatalytic performance of ZnO nanomaterials for self sensitized degradation of malachite green dye under solar light. Applied Catalysis A: General. 2015;490:42-49.
44. Sahoo A, Dixit T, Kumari A, Gupta S, Kothandaraman R, Rajeev PP, et al. Facile control of giant green-emission in multifunctional ZnO quantum dots produced in a single-step process: femtosecond pulse ablation. Nanoscale Advances. 2025;7(2):524-535.
45. Venhryn YI, Serednytski AS, Korniy SA, Popovych DI, Mudry SI. Photoluminescent properties in different gas ambient of ZnO nanopowders doped by Mo and V. Applied Nanoscience. 2023;13(12):7631-7636.
46. Akazawa H. Defect species in Ga-doped ZnO films characterized by photoluminescence. Journal of Vacuum Science and Technology A: Vacuum, Surfaces, and Films. 2021;39(3).
47. Sledd J. [kut] [kut] Be [kut], [kut] It? American Speech. 1993;68(2):218.
48. Hattori Y, Mukasa S, Toyota H, Inoue T, Nomura S. Synthesis of zinc and zinc oxide nanoparticles from zinc electrode using plasma in liquid. Mater Lett. 2011;65(2):188-190.
49. Saito G, Hosokai S, Akiyama T. Synthesis of ZnO nanoflowers by solution plasma. Materials Chemistry and Physics. 2011;130(1-2):79-83.